Field induced phase transitions in the helimagnet $Ba_2CuGe_2O_7$

J. Chovan[1,*], M. Marder[2,†] and N. Papanicolaou[3,‡]
[1] *Department of Physics, Matej Bel University, Banská Bystrica, Slovakia**
[2] *Center for Nonlinear Dynamics and Department of Physics, The University of Texas at Austin, Austin, Texas 78712* † *and*
[3] *Department of Physics and Institute of Plasma Physics, University of Crete, Heraklion, Greece*‡

(Dated: November 27, 2012)

Abstract. We present a theoretical study of magnetic properties of the two-dimensional spiral antiferromagnet $Ba_2CuGe_2O_7$ in the presence of an external magnetic field. Some time ago we predicted that when a field is applied parallel to the c axis, a previously anticipated Dzyaloshinskii-type incommensurate–to–commensurate phase transition is actually mediated by an *intermediate phase*. This phase was recently observed in experiments where magnetic fields were nearly parallel to the c axis and referred to as a *double-k structure*. Here we calculate the low-energy magnon spectrum throughout the phase transition, verifying stability of the intermediate phase, and providing the opportunity for comparison with inelastic neutron scattering. In addition, we calculate the $T = 0$ phase diagram for arbitrary canted magnetic fields, in general agreement with experiment. In particular we show that a weakly broken $U(1)$ symmetry of our model accounts for sudden $\pi/2$ rotations of the magnetic structures observed in experiment. Finally, our analysis suggests a nonzero weak-ferromagnetic component in the underlying Dzyaloshinskii-Moriya anisotropy, which is not crucial for the appearance of the double-k structure, but is important to restore quantitative agreement with experiment.

PACS numbers: 75.30.Ds, 75.30.Gw, 75.30.Kz

I. INTRODUCTION

The presence of Dzyaloshinskii-Moriya (DM) anisotropy[1,2] in low-symmetry magnetic crystals typically leads to weak ferromagnetism, as a result of slight spin canting in an otherwise antiferromagnetic (AF) ground state. Another possibility is the occurrence of helimagnetism whereby spins are arrayed in a helical or spiral structure whose period (pitch) extends over several decades of unit cells. $Ba_2CuGe_2O_7$ is an example of a helimagnet which has proved to be especially well suited for experimental investigation thanks to a fortunate combination of physical properties. It is an insulator whose magnetic properties can be understood in terms of localized $s = \frac{1}{2}$ spins carried by the Cu^{2+} ions. The scale of energy set by an exchange constant $J \sim 1$ meV is very convenient for neutron scattering experiments. Because of the low tetragonal symmetry (space group $P\bar{4}2_1m$) the corresponding Heisenberg Hamiltonian involves an interesting combination of antisymmetric (DM) as well as symmetric exchange anisotropies which lead to a rich phase diagram. In particular, the strength of anisotropy is such that magnetic phase transitions take place at critical fields that are well within experimental reach.

Indeed, a series of experiments in the late nineties[3–7] revealed the existence of a Dzyaloshinskii-type[8] incommensurate-to-commensurate (IC) phase transition when the strength of an external field applied along the c axis exceeds a critical value, $H_c \sim 2$ T. For $H < H_c$ the ground state is an incommensurate spiral whose period $L = L(H)$ grows to infinity in the limit $H \to H_c$. For $H > H_c$ the ground state was thought to become a commensurate antiferromagnetic spin-flop state. We also note that the Dzyaloshinskii-type transition is similar to the cholesteric-nematic phase transition induced by an external magnetic field in chiral liquid crystals[9–11].

However, a detailed theoretical investigation[12–14] inspired by the earlier experimental work[3–7] predicted that the IC phase transition does not occur immediately, and that, instead, between the incommensurate and commensurate phases occurs a separate *intermediate phase*. In short, there exist two critical fields, H_{c1} and H_{c2} such that $H_{c1} < H_c < H_{c2}$ where $H_c \sim 2$ T is the critical field for the presumed Dzyaloshinskii-type phase transition. For $H < H_{c1} \sim 1.7$ T the ground state is a flat spiral (cycloid) that propagates along the x axis while the staggered magnetization rotates in the xz plane. For $H > H_{c1}$ the cycloid transforms into a nonflat spiral where all three components of the staggered magnetization are different from zero (Fig. 1). Such a state may concisely be described as an antiferromagnetic conical spiral that propagates along the x axis while it nutates around the y axis. When the field approaches a second critical value, $H_{c2} \sim 2.9$ T the antiferromagnetic cone degenerates into a uniform state whose staggered magnetization points along the y axis modulo an azimuthal rotation. This state is a commensurate antiferromagnetic spin-flop state which is the ground state for all $H > H_{c2}$. Therefore the Dzyaloshinskii field H_c is not a true critical field, and the corresponding IC phase transition is actually mediated by an additional phase in the region $H_{c1} < H < H_{c2}$.

This prediction[12] remained unexplored for almost a decade. However a new series of experiments has now confirmed the occurrence of an intermediate phase in the form of an antiferromagnetic conical spiral which has been called a *double-k structure* by the experimental dis-

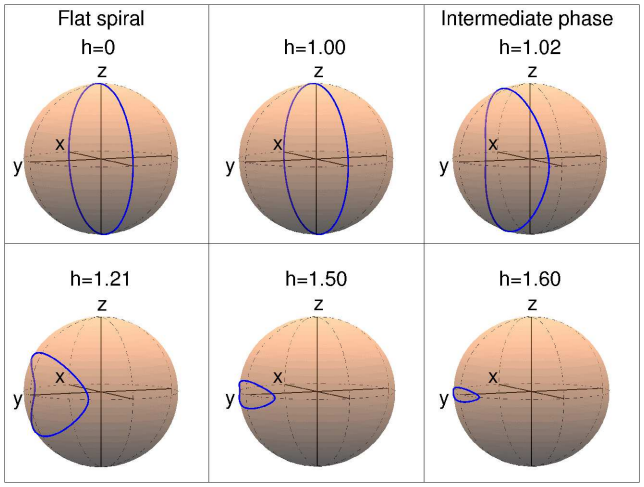

Figure 1. (Color online) Diagrams illustrating the forms of various spiral states for differing values of magnetic field h in units of 1.68 T along the c axis. Blue lines on the sphere surface trace out directions for the staggered magnetization, placing the base of each $\mathbf{n}$ at the center of the sphere and then moving from one unit cell to the next along x, the direction of spiral propagation. For $0 < h < h_{c1}$ the spins describe a cycle in the xz plane, while for $1 < h < h_{c2} = \sqrt{3}$ they also have a nonzero oscillating y component.

coverers. This state occurs as predicted when an external magnetic field is applied almost perfectly parallel to the c axis[16], while further experiments have also explored the $T = 0$ phase diagram in the presence of an arbitrary canted magnetic field[17]. Our current task is to confirm that the recently observed double-k structure is indeed the intermediate phase predicted in Ref. 12 and further to calculate the phase diagram in arbitrary canted magnetic fields so as to complete the connection with the latest experiments.

In the method of calculation we closely follow the work of Ref. 12. We first note that $Ba_2CuGe_2O_7$ is a layered compound where the Cu atoms form a perfect square lattice within each layer. The interaction between out-of-plane neighbors is ferromagnetic and weak. Therefore the inter layer coupling is ignored in the following discussion which concentrates on the two-dimensional dynamics within each layer. The low-energy dynamics is then calculated in terms of a suitable variation of the nonlinear σ model governed by Lagrangian density $\mathcal{L}$:

$$\begin{aligned} \mathcal{L} &= \mathcal{L}_0 - V; \qquad (1)\\ \mathcal{L}_0 &= \frac{1}{2}\partial_0\mathbf{n}\cdot\partial_0\mathbf{n} + \mathbf{h}\cdot\mathbf{n}\times\partial_0\mathbf{n};\\ V &= \frac{1}{2}\left(\partial_1\mathbf{n} - \mathbf{e}_2\times\mathbf{n}\right)^2 + \frac{1}{2}\left(\partial_2\mathbf{n} - \mathbf{e}_1\times\mathbf{n}\right)^2\\ &\quad + \frac{1}{2}(\mathbf{n}\cdot\mathbf{h})^2 + d_z(\mathbf{h}\times\mathbf{e}_3)\cdot\mathbf{n}. \end{aligned}$$

Here $\mathbf{e}_1$, $\mathbf{e}_2$, and $\mathbf{e}_3$ are unit vectors along the x, y, and z axes and $\mathbf{n} = n_1\mathbf{e}_1 + n_2\mathbf{e}_2 + n_3\mathbf{e}_3$ is the staggered magnetization which is a unit vector field that depends upon the in-plane spatial coordinates x and y as well as the time variable t: $\mathbf{n} = \mathbf{n}(x, y, t)$. Accordingly, derivatives are described by $\partial_1 = \partial/\partial x$, $\partial_2 = \partial/\partial y$, and $\partial_0 = \partial/\partial t$. The applied magnetic field $\mathbf{h} = h_1\mathbf{e}_1 + h_2\mathbf{e}_2 + h_3\mathbf{e}_3$ may point in any arbitrary direction. It should be noted that anisotropy has been restricted to the special KSEA limit by setting $\kappa = 0$ in the Lagrangian of Ref. 12. Otherwise Eq. (1) gives the most general Lagrangian compatible with symmetry, expressed in fully rationalized units. Specifically, frequency is measured in units of $\hbar\omega = 0.24$ meV, distance in units of 33.75 Å and magnetic field in units of 1.68 T. The remaining free parameter $d_z = \sqrt{2}D_z/D_\perp$ is a dimensionless ratio of the out-of-plane component of the DM anisotropy D_z and its in-plane component $D_\perp$. The latter has been completely suppressed in Eq. (1) except through the definitions of rationalized units quoted above.

The ground state properties and the associated low-energy dynamics will be calculated from Eq. (1) for a magnetic field of varying strength and direction. Hence, in Sec. II the field is restricted to point along the c (or z) axis and its strength is varied through the IC transition. We recover the results of Ref. 12 and complete an explicit calculation of the low-energy magnon spectrum throughout the intermediate phase. In Sec. III we study the case of a field applied in a direction perpendicular to the c axis. We thus recover the experimentally observed bisection rule and further illuminate the role of the out-of-plane DM anisotropy d_z. The case of a magnetic field applied in an arbitrary direction (canted magnetic field) is analyzed in Sec. IV where we present a theoretical prediction for the $T = 0$ phase diagram, in fair agreement with recent experiments. Finally our main conclusions are summarized in Sec. V.

II. FIELD PARALLEL TO c

We begin by specializing to the case where the magnetic field is applied strictly along the c axis: $\mathbf{h} = h\mathbf{e}_3$. Then the potential V of Eq. (1) reduces to

$$\begin{aligned} V = \frac{1}{2}\Big[(\partial_1\mathbf{n})^2 + (\partial_2\mathbf{n})^2 + \left(1+h^2\right)n_3^2 + 1\Big]\\ - \left[\left(\partial_1 n_1 - \partial_2 n_2\right)n_3 - \left(n_1\partial_1 - n_2\partial_2\right)n_3\right] \qquad (2) \end{aligned}$$

and is symmetric under the $U(1)$ transformation

$$x + iy \to (x+iy)\,e^{i\psi}, \quad n_1 + in_2 \to (n_1+in_2)\,e^{-i\psi}, \qquad (3)$$

which is somewhat unusual in that an azimuthal rotation of spatial coordinates x and y by an angle ψ is followed by a corresponding rotation of the staggered magnetization by an angle $-\psi$.

The ground state is obtained by finding energy-minimizing solutions $\mathbf{n}$ of the static energy functional

$$W = \int dx\,dy\,V. \qquad (4)$$

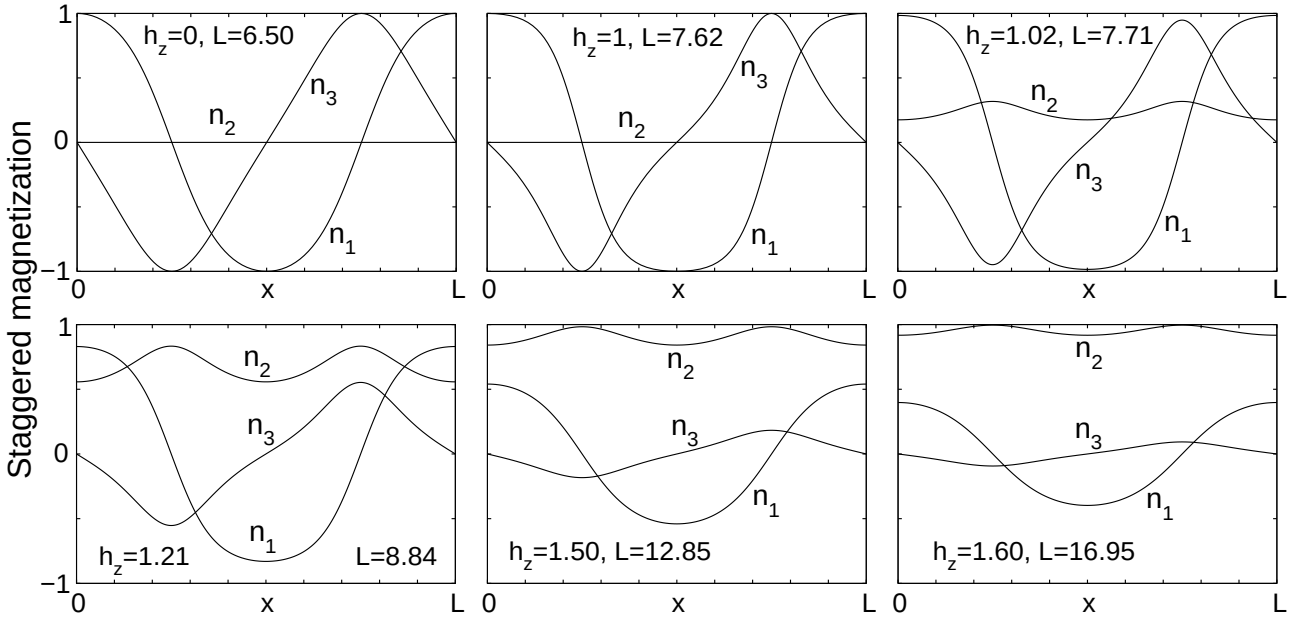

Figure 2. Solutions of Eqs. (7) minimizing the average energy density of Eq.(15) for a number of illustrative magnetic fields $h = h_z$ pointing along the c axis. Note that the period L varies with the field.

In order to enforce the constraint that the staggered magnetization be of unit length we adopt a parameterization

$$\mathbf{n} = \sin\Phi \sin\Theta\, \mathbf{e}_1 + \cos\Theta\, \mathbf{e}_2 + \cos\Phi \sin\Theta\, \mathbf{e}_3, \quad (5)$$

which differs from more standard parameterizations by a circular permutation, but turns out to yield slightly more compact expressions later on.

Our first task to to find solutions $\Theta = \Theta(x, y)$, $\Phi = \Phi(x, y)$ that minimize W. Extensive two-dimensional simulations yielded negative results for a potential ground state in the form of, say, a vortex lattice. On the other hand, nontrivial results are obtained by restricting both Θ and Φ to be functions of x alone:

$$\Theta(x, y) = \theta(x); \quad \Phi(x, y) = \phi(x). \quad (6)$$

In view of the $U(1)$ symmetry in Eq. (3) any solution we find of this type automatically produces a family of additional solutions of the same energy rotated by angle ψ. Varying W then yields

$$\partial_1^2\phi = -\frac{(2\,\partial_1\phi - 2)\,\cos\theta\,\partial_1\theta + \gamma^2\,\cos\phi\,\sin\phi\,\sin\theta}{\sin\theta}$$

$$\partial_1^2\theta = \Big((\partial_1\phi)^2 - 2\,\partial_1\phi + \gamma^2\,\cos^2\phi\Big)\,\cos\theta\,\sin\theta. \quad (7)$$

with $\gamma^2 = 1 + h^2$. Here subscript 1 indicates a derivative with respect to x. All derivatives with respect to y vanish because we are working in a space of one-dimensional solutions.

To illustrate the solutions, we first consider the special case of a *flat spiral* (cycloid) with $\theta = \pi/2$. Then the second of Eqs. (7) is automatically satisfied and the first becomes

$$\partial_1^2\phi + \gamma^2 \cos\phi \sin\phi = 0, \quad (8)$$

while the staggered magnetization becomes

$$\mathbf{n} = (\sin\phi, 0, \cos\phi), \quad (9)$$

a cycloid that propagates along the x axis while rotating in the xz plane (upper left panel of Fig. 1). The solution for ϕ obeys

$$\partial_1\phi = \sqrt{\delta^2 + \gamma^2\cos^2\phi}, \quad x = \int_0^\phi \frac{d\varphi}{\sqrt{\delta^2 + \gamma^2\cos^2\varphi}}. \quad (10)$$

The result can be expressed in terms of elliptic functions but there is no particular advantage to doing so. δ^2 is a positive constant that will be determined below. The cycloid has a period (pitch) of

$$L = \int_0^{2\pi} \frac{d\phi}{\sqrt{\delta^2 + \gamma^2\cos^2\phi}} \quad (11)$$

and the free parameter δ is determined by the requirement that the average energy density $w = W/L$ achieve a minimum:

$$\frac{1}{2\pi}\int_0^{2\pi} d\phi\sqrt{\delta^2 + \gamma^2\cos^2\phi} = 1 \Rightarrow w = \frac{1}{2}(1 - \delta^2). \quad (12)$$

As γ (or h) increases δ becomes zero at a critical field:

$$\gamma = \gamma_c = \pi/2 \Rightarrow h = h_c = \sqrt{\frac{\pi^2}{4} - 1} \approx 1.21. \quad (13)$$

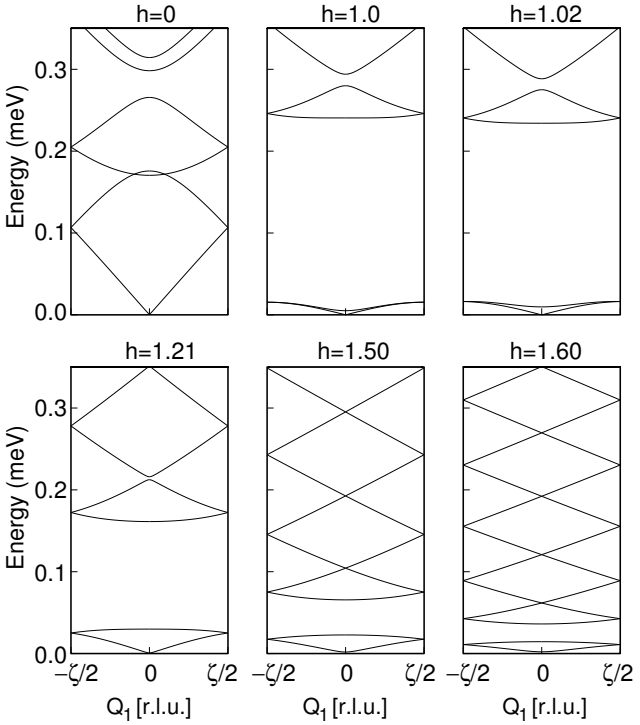

Figure 3. Magnon spectrum along the x direction in the reduced zone scheme for six illustrative magnetic fields. For $h > h_{c1} = 1.01$ the results show the magnon spectrum of the intermediate phase. The wave number Q_1 is measured in relative lattice units defined in Ref. 12. Note that the lowest-lying band has a linear dispersion relation.

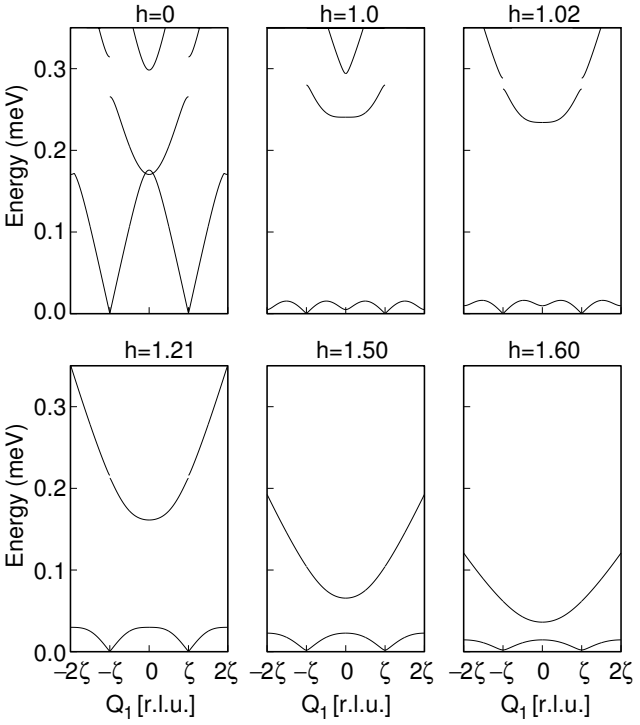

Figure 4. Magnon spectrum along the x direction in the extended zone scheme for six illustrative magnetic fields. For $h > h_{c1} = 1.01$ the results show the magnon spectrum of the intermediate phase. Bands have been assembled in a fashion that corresponds with conventions in publication of experiments.

In physical units, $H_c = 2.04$ T. This is the Dzyaloshinskii critical field and the corresponding Dzyaloshinskii scenario may be described as follows: for $h < h_c$ the solution is a flat spiral that propagates along the x axis and rotates in the xz plane. As h approaches h_c the spiral is highly distorted and becomes a kink-like structure with diverging period. For $h > h_c$ the ground state becomes the uniform spin-flop state

$$\mathbf{n} = (1, 0, 0) \quad \text{modulo } U(1).$$

We realized that this scenario was incomplete when we computed the magnon spectrum[12] of the flat spiral and found negative eigenvalues starting at

$$h_{c1} = 1.01, \quad H_{c1} = 1.7 \text{ T}. \tag{14}$$

Above this value the flat spiral is unstable. We thus return to energy minimization and revoke the assumption $\theta = \pi/2$, although continuing to assume a one-dimensional structure of the form $\phi = \phi(x)$ and $\theta = \theta(x)$.

Efforts to find explicit analytical solutions of Eqs. (7) have not been fruitful so we resort to numerics. We minimize the energy density

$$w = \frac{1}{L} \int_0^L dx\, V(\theta, \phi) \tag{15}$$

over a periodic chain of length L and vary L to achieve a minimum for any given value of h.

For $h < h_{c1} = 1.01$ we recover the previous results for the flat spiral. But for $h > h_{c1}$ a nonflat spiral arises with nontrivial $\phi(x)$ as well as $\theta(x)$. We emphasize again that our numerical investigations of more general two-dimensional structures have never yielded lower energies. Examples appear in Fig. 2 for a variety of field values. Entering the intermediate phase for $h > h_{c1}$, n_2 acquires nonzero values and one can describe the state as an antiferromagnetic conical spiral that propagates along x but nutates around y. This is precisely the structure deduced from recent scattering experiments[16,17] and called a *double-k structure* because of two-fold peak characteristically observed during experimental scans through k space. As h increases, the component n_2 becomes larger and larger until at $h_{c2} = \sqrt{3}$ (or $H_{c2} = 2.9$ T) the solution becomes a spin-flop state with $\mathbf{n} = (0, 1, 0)$. This upper critical point was determined in Ref. 12 from a stability analysis of the spin-flop state. The existence of the intermediate state does not depend upon the presence of a nonzero transverse magnetic field.

We now proceed to obtain the magnon spectrum of the intermediate state. We consider perturbations in the

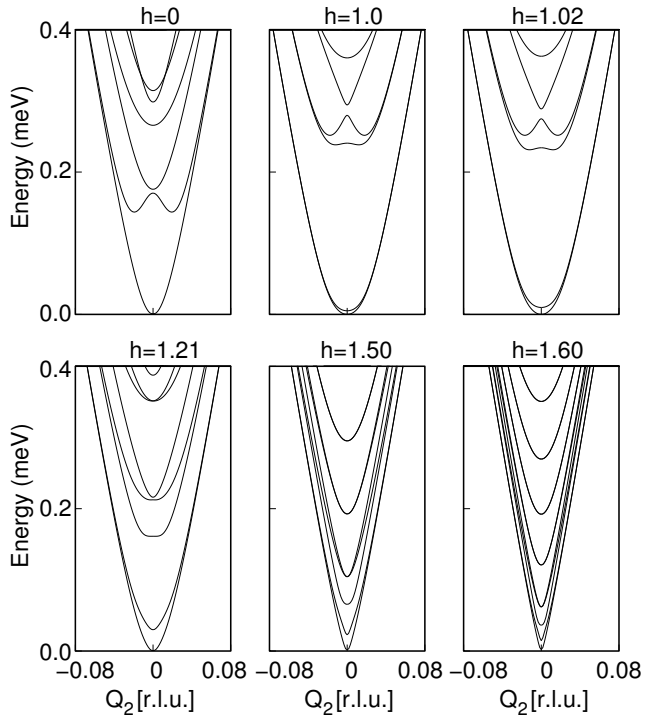

Figure 5. Magnon spectrum along the y direction for six illustrative magnetic fields. For $h > h_{c1} = 1.01$ the results show the magnon spectrum of the intermediate phase. The wave number Q_2 is measured in relative lattice units defined in Ref. 12.

form

$$\Theta(x,y,t) = \theta(x) - g(x,y,t)$$
$$\Phi(x,y,t) = \phi(x) + f(x,y,t)/\sin\theta(x) \qquad (16)$$

where θ and ϕ are solutions for the intermediate state found previously. Then working to linear order in f, g

$$(\partial_1^2 + \partial_2^2 - \partial_0^2) f = U_{11} f + U_{12} g + A\partial_1 g + B\partial_2 g + C\partial_0 g$$
$$(\partial_1^2 + \partial_2^2 - \partial_0^2) g = U_{22} g + U_{21} f - A\partial_1 f - B\partial_2 f - C\partial_0 f \qquad (17)$$

where all functions except f and g are functions only of x and are given by

$$U_{11} = -(\partial_1\theta)^2 + \cos^2\theta\left((\partial_1\phi)^2 - 2\,\partial_1\phi\right) + \gamma^2\left(\cos^2\phi\,\cos^2\theta - 2\,\cos^2\phi + 1\right)$$

$$U_{12} = -\frac{(2\,\partial_1\phi - 2)\,\partial_1\theta}{\sin\theta}$$

$$U_{21} = \frac{(2\,\partial_1\phi - 2)\,\cos^2\theta\,\partial_1\theta + 2\,\gamma^2\,\cos\phi\,\sin\phi\,\cos\theta\,\sin\theta}{\sin\theta}$$

$$U_{22} = -\left((\partial_1\phi)^2 - 2\,\partial_1\phi + \gamma^2\,\cos^2\phi\right)\left(2\,\sin^2\theta - 1\right)$$

$$A = (2\,\partial_1\phi - 2)\,\cos\theta$$

$$B = -2\,\sin\phi\,\sin\theta$$

$$C = -2\,h\,\cos\phi\,\sin\theta. \qquad (18)$$

We have verified that for the flat spiral ($\theta = \pi/2$, $\partial_1\phi = \sqrt{\delta^2 + \gamma^2\cos^2\phi}$) these expressions reduce to those previously obtained for the magnon spectrum of the flat spiral in Eq. (5.2) of Ref. 12, but with $\phi \longleftrightarrow \theta$.

We have solved the linear system (17) by a Bloch analysis of the type given in Appendix A of Ref. 12 now extended to calculate the low-energy magnon spectrum throughout the intermediate phase $h_{c1} < h < h_{c2}$. We present the results of the magnon calculations in Figs. 3 through 5. We make the following comments:

- All eigenvalues are positive. Therefore the intermediate state is locally stable. This computation does not prove it is the ground state, but in combination with extensive numerical explorations of two-dimensional states that found no solutions of lower energy, it is a strong indication.

- We provide plots both in the reduced zone scheme and the extended zone scheme. The reduced zone scheme is more compact, particularly for h_{c1} and below. However as the field increases towards h_{c2} the reduced zone scheme acquires a large number of bands that are resolved more clearly in the extended zone scheme. Experimentalists are likely to find the display in the extended zone scheme more useful.

- Along Q_1 the low-energy spectrum is linear at the zone center. Moving towards h_{c2} it acquires two bands, an 'acoustic' band with linear dispersion and an upper optical band (higher bands exist that have not been resolved by the computation). The linear portion of the acoustic band is the Goldstone mode of these magnetic spin states. In the limit that $h \to h_{c2}$ the bands depicted here collapse onto the horizontal axis; the next excitation is at an energy over 0.4 that lies above the top of the figure.

- Along Q_2 the low-energy spectrum is quadratic. As h increases towards h_{c2} the quadratic regions become small and the spectrum becomes nearly linear. Upon reaching h_{c2}, the dispersion becomes completely linear. At this point it produces the Goldstone mode of the spin-flop phase.

III. FIELD PERPENDICULAR TO c

We next consider a field applied in a direction strictly perpendicular to the c axis, a case that had attracted experimental interest already in Ref. 6. For the moment, we assume that the field is applied along the y axis, $\mathbf{h} =$

$(0, h_\perp, 0)$, hence the potential V of Eq. (1) reduces to

$$V = \frac{1}{2}\left[(\partial_1 \mathbf{n})^2 + (\partial_2 \mathbf{n})^2 + n_3^2 + h_\perp^2 n_2^2 + 1\right] + h_\perp d_z n_1 - \left[(\partial_1 n_1 - \partial_2 n_2)\, n_3 - (n_1 \partial_1 - n_2 \partial_2)\, n_3\right], \qquad (19)$$

where the applied field enters in two distinct ways; namely through the appearance of an effective easy-plane anisotropy $\frac{1}{2}h_\perp^2 n_2^2$ and a Zeeman-like anisotropy $h_\perp d_z n_1$. The latter also contains the strength d_z of the out-of-plane oscillating component ($\pm D_z$) of the DM vectors which was neglected in the analysis of Ref. 6.

To find minima of the energy functional we first note that the positive term $\frac{1}{2}h_\perp^2 n_2^2$ again favors a flat-spiral configuration with $n_2 = 0$ which propagates along the x axis. Using the angular parametrization (5) we write

$$\Phi = \phi\,(x)\ , \quad \Theta = \frac{\pi}{2}\,; \quad \mathbf{n} = (\sin\phi,\, 0,\, \cos\phi)\ , \qquad (20)$$

which is inserted in Eq. (19) to yield

$$V = \frac{1}{2}\left[(\partial_1\phi - 1)^2 + \cos^2\phi\right] + \bar{h}\sin\phi\,, \qquad (21)$$

where the only free parameter

$$\bar{h} = h_\perp d_z \qquad (22)$$

is a combination of the applied field $h_\perp$ and the effective out-of-plane DM anisotropy d_z.

Otherwise, the calculation is similar to that of the flat spiral in Sec. II. Stationary points of the energy functional $W = \int V dx$ now satisfy the ordinary differential equation

$$\partial_1^2\phi + \cos\phi\sin\phi - \bar{h}\cos\phi = 0 \qquad (23)$$

whose first integral is given by

$$(\partial_1\phi)^2 - \cos^2\phi - 2\bar{h}\sin\phi = C = 2\bar{h} + \delta^2\,. \qquad (24)$$

Our choice of the integration constant C indicates that minimum energy is achieved with a positive new constant denoted by δ^2. The actual configuration $\Phi = \phi\,(x)$ is then given by the implicit equation

$$x = \int_0^\phi \frac{d\varphi}{\sqrt{\delta^2 + \cos^2\varphi + 2\bar{h}(1+\sin\varphi)}}\,, \qquad (25)$$

and the corresponding spiral period L is given by

$$L = \int_0^{2\pi} \frac{d\phi}{\sqrt{\delta^2 + \cos^2\phi + 2\bar{h}(1+\sin\phi)}}\,. \qquad (26)$$

Finally, the free parameter δ^2 is calculated by minimizing the average energy density $w = \frac{1}{L}\int_0^L V(x)dx$ which yields

$$\frac{1}{2\pi}\int_0^{2\pi} d\phi\sqrt{\delta^2 + \cos^2\phi + 2\bar{h}(1+\sin\phi)} = 1\,, \qquad (27)$$

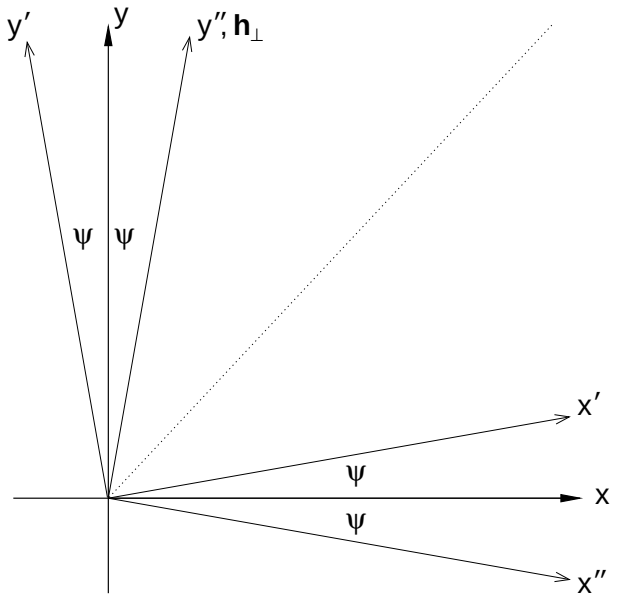

Figure 6. Illustration of the bisection rule in a transverse field applied along the y'' axis. The spiral propagation vector points along the x' axis, while the staggered magnetization rotates in the $x''z$ plane.

an algebraic equation that may be used to determine δ^2 for each value of $\bar{h}$. The corresponding minimum energy is then given by

$$w = \frac{1}{2}(1 - \delta^2 - 2\bar{h}). \qquad (28)$$

In the absence of the out-of-plane DM anisotropy ($d_z = 0$) the configuration just calculated reduces to the zero-field flat spiral of Sec.II for any value of the applied transverse field because $\bar{h} = h_\perp d_z = 0$ for all $h_\perp$. In particular, no phase transition of the Dzyaloshinskii type would be expected to occur for a field applied in a direction strictly perpendicular to the c axis, as presumed in the analysis of early experiments[6].

However, the situation changes significantly for $d_z \neq 0$. Then the effective field $\bar{h} = h_\perp d_z$ is different from zero except when $h_\perp = 0$. With increasing $h_\perp$, and thus increasing $\bar{h}$, the parameter δ^2 decreases and eventually vanishes when $\bar{h}$ reaches a critical value $\bar{h} = \bar{h}_c$ computed from Eq. (26) applied for $\delta^2 = 0$. A simple numerical calculation yields $\bar{h}_c = h_\perp^c d_z = 0.3161$, or

$$h_\perp^c = \frac{0.3161}{d_z}\,. \qquad (29)$$

In the limit $h_\perp \to h_\perp^c$, δ^2 vanishes and the average energy density of Eq. (28) reduces to $w = \frac{1}{2}(1 - 2\bar{h}_c)$ which coincides with the energy of the uniform spin-flop state $\mathbf{n} = (-1, 0, 0)$. Thus we again encounter a Dzyaloshinskii-type phase transition at a critical field that now depends on d_z.

As mentioned already, no such transition was detected in the early experiments[6] which were conducted with

transverse magnetic fields of limited strength $H_\perp \lesssim 2$ T or $h_\perp \lesssim 2/1.68 \approx 1.2$. However, recent experiments[17] reveal a critical field $H_\perp^c = 9$ T or $h_\perp^c = 9/1.68 = 5.36$ and, using Eq. (29),

$$d_z = 0.06. \tag{30}$$

As far as we know, this is the first estimate of the strength of the out-of-plane DM anisotropy and will be used in all numerical calculations presented in the continuation of this paper. Incidentally, using the definition of the rationalized anisotropy $d_z = \sqrt{2}D_z/\varepsilon J$ from Ref. 12, we find $D_z/J = 0.0076$, to be compared with $\varepsilon = D_\perp/J = 0.18$.

The preceding calculation was completed in Ref. 13 with a detailed calculation of the corresponding magnon spectrum which could prove useful for the analysis of future inelastic neutron scattering experiments in the presence of a strong transverse magnetic field $H_\perp$. The same calculation reveals no sign of further critical instabilities as long as $d_z < 0.5$. In particular, an intermediate phase of the type encountered in Sec. II is not present in the case of strictly transverse magnetic fields and $d_z < 0.5$. In other words, the predicted phase transition is of pure Dzyaloshinskii type[8].

This section is completed with a brief discussion of the case of a transverse magnetic field

$$\mathbf{h}_\perp = h_\perp \left(\sin\psi, \cos\psi, 0\right) \tag{31}$$

which points in an arbitrary direction within the basal plane obtained by a clockwise rotation of the y axis with angle ψ (see Fig. 6). In fact, the ground-state configuration for this more general case ($\psi \neq 0$) can be surmised from the special $\psi = 0$ solution calculated earlier in this section by simple algebraic transformations, thanks to the underlying $U(1)$ symmetry of Eq. (3) broken by the applied transverse field. Indeed, let $n_1 = n_1(x), n_2 = 0, n_3 = n_3(x)$ be the $\psi = 0$ solution. Then the solution for $\psi \neq 0$ is given by

$$n_1' = \cos\psi\, n_1(\xi)\,, \quad n_2' = -\sin\psi\, n_1(\xi)\,, \quad n_3' = n_3(\xi)\,, \tag{32}$$

where $\xi = x\cos\psi + y\sin\psi$. Thus the new spiral propagates along the x' axis obtained by a counter-clockwise rotation of the x axis with angle ψ (see Fig. 6) while the staggered magnetization rotates in the plane $x''z$ which is perpendicular to the field direction (axis y''). In other words, a flat spiral (cycloid) that initially propagates along the x axis and rotates in the xz plane ($\psi = 0$) is reoriented to propagate along the x' axis ($\psi \neq 0$) so that the normal to the spin plane (axis y'') points along the applied magnetic field. The angle formed by the direction of spiral propagation (axis x') and the normal to the spin plane (axis y'') is bisected by the conventional crystal axis $b = (0, 1, 0)$ denoted by a dotted line in Fig. 6 for any ψ. When the field is applied along b, $\psi = \frac{\pi}{4}$ and the normal to the spin-rotation plane is parallel to the propagation vector (screw-type spiral).

The "bisection rule" just described theoretically was experimentally discovered already in Ref. 6. Actually, agreement with the ideal bisection rule requires that $H_\perp \gtrsim 0.5$ T in order to overcome a certain energy barrier due to discreteness effects which lead to an additional tetragonal anisotropy that breaks the underlying $U(1)$ symmetry even in the absence of a transverse field[6,15]. The same anisotropy explains the experimental fact that the spiral propagates along the $x = (1, 1, 0)$ or $x = (1, \bar{1}, 0)$ directions, in the absence of a transverse field, while a sufficiently strong field $H_\perp \gtrsim 0.5$ T is required to reorient the spiral according to the bisection rule.

We have thus completed the discussion of the phase diagram in the presence of a field strictly parallel to the c axis (Sec. II) or a field strictly perpendicular to c (Sec. III). The general case of a canted magnetic field is discussed in the following Sec. IV.

IV. CANTED MAGNETIC FIELDS

We now turn our attention to the most general case of the applied field $\mathbf{h}$, whose transverse component $h_\perp$ and the component h_z along the c axis are both nonzero. For a while we assume that the magnetic field $\mathbf{h}$ is given by

$$\mathbf{h} = h_\perp \mathbf{e}_2 + h_z \mathbf{e}_3\,. \tag{33}$$

The explicit form of the potential of Eq. (1) becomes

$$\begin{aligned} V = \frac{1}{2}\left[(\partial_1\mathbf{n})^2 + (\partial_2\mathbf{n})^2 + 1\right] - \\ - \left[(\partial_1 n_1 - \partial_2 n_2)\, n_3 - (n_1\partial_1 - n_2\partial_2)\, n_3\right] \\ + \frac{1}{2}\gamma^2 n_3^2 + \frac{1}{2}h_\perp^2 n_2^2 + h_\perp h_z n_2 n_3 + h_\perp d_z n_1\,, \end{aligned} \tag{34}$$

where the parameter γ^2 depends upon h_z,

$$\gamma^2 = 1 + h_z^2. \tag{35}$$

When $h_\perp \neq 0$, a brief inspection of the potential of Eq. (34) reveals that the Zeeman energy $\frac{1}{2}(\mathbf{n}\cdot\mathbf{h})^2$ now contains also the *off-diagonal* anisotropy $h_\perp h_z n_2 n_3$, which was absent when either $h_\perp = 0$ or $h_z = 0$. The presence of the latter anisotropy precludes analytical treatment. We therefore obtain the corresponding solutions by a direct minimization of the energy functional, in a manner analogous to the calculation presented in Sec. II. We state our results in the phase diagram in Fig. 7.

We begin our discussion with the case where $h_z < h_{c1} = 1.01$ (or $H_z < H_{c1} = 1.7$ T). and consider the evolution of the system with increasing $h_\perp$. Our results are displayed in Fig. 8(a). In the limit $h_\perp = 0$, shown in the top entry, the spin configuration that minimizes the energy is the flat spiral constructed in Sec. II. Recall that this solution is degenerate with respect to rotations around c, in agreement with the $U(1)$ symmetry given by Eq. (3). When $h_\perp \neq 0$, our results make it clear that the

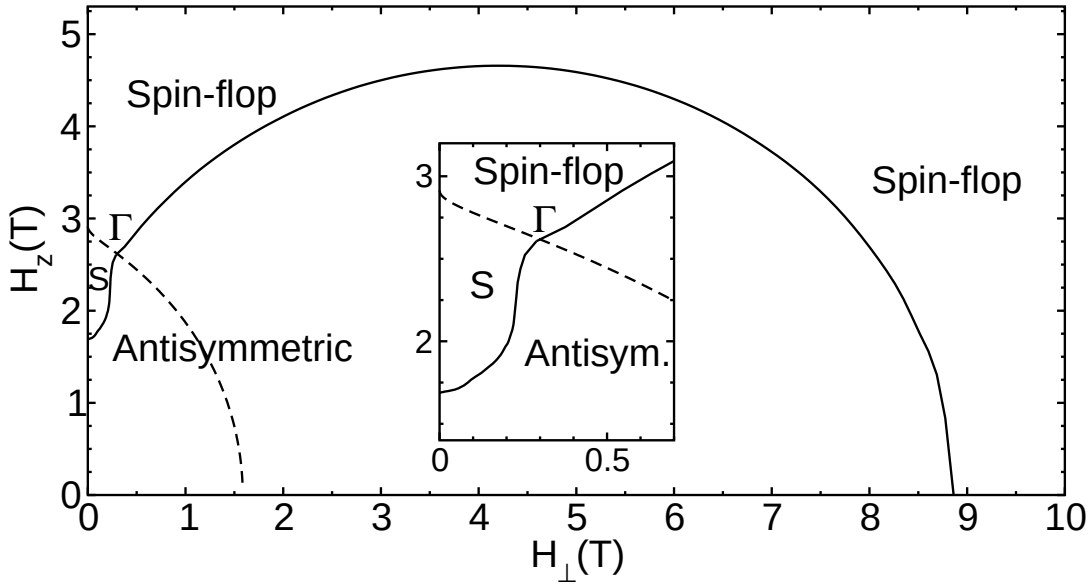

Figure 7. Theoretical prediction for the phase diagram. We adopted conventions used in publication of experiments[17]. The Antisymmetric phase is realized below the solid line. The Symmetric phase, denoted as S in the figure, exists in the area between the solid line and the dashed line. The dashed line depicts the limit of local stability of the Spin-flop phase. The Spin-flop phase is locally stable above the dashed line, but is actually realized only in the area above both the dashed line and the solid line. The inset emphasizes the region near the tricritical point Γ where the three phases (Symmetric, Antisymmetric, Spin-flop) merge.

energy is minimized by a nonflat spin spiral propagating along the x axis. The component of the staggered magnetization n_2 is now different from zero and points in the direction of the transverse field $h_\perp$, and its sign oscillates over the period $L = L(h_z, h_\perp)$. Because of this characteristic behavior, we call this state the *Antisymmetric phase*. The origin of the oscillating component n_2 can be understood by a direct inspection of the Zeeman energy $\propto (\mathbf{n}\cdot\mathbf{h})^2$. Its diagonal terms $n_2^2 h_\perp^2$, $n_3^2 h_z^2$ are always positive, but the off-diagonal contribution may become *negative* provided that n_2 adjusts so that its sign is always opposite to the sign of n_3. Because the sign of n_3 oscillates (the projection of $\mathbf{n}$ onto the xz plane rotates during the period L), n_2 also displays oscillatory behavior. To fully describe the spin structure, all terms in the potential of Eq. (34) must be considered, but the main conclusion persists – the spiral minimizes its energy by developing $n_2 \neq 0$ *along the direction of the transverse field* $h_\perp$, and the sign of n_2 oscillates over the period L. As a result, the expectation value $\langle n_2 n_3\rangle$ becomes negative ($\langle n_2 n_3\rangle < 0$), while $\langle n_2\rangle = \langle n_3\rangle = 0$, as verified by a direct calculation.

We now briefly describe the role of the term $h_\perp d_z n_1$ in Eq. (34). The importance of the latter contribution has already been established in Sec. III during our analysis of the properties of the flat spiral ($n_2 = 0$) in the presence of a field applied strictly in the xy plane ($h_\perp \neq 0$, but $h_z = 0$). The scenario discussed in Sec. III is here mildly modified by the presence of $h_z \neq 0$ but it main features remain the same, as confirmed by our numerical studies. The weak–ferromagnetic anisotropy $h_\perp d_z n_1$, generated by the transverse field $h_\perp$ *applied along the* y *axis*, makes the spin orientations along the $\pm x$ axis energetically nonequivalent. In the Antisymmetric state, the component of the staggered magnetization that is perpendicular to the transverse field $h_\perp$ rotates in the xz plane, and is thus directly affected by the weak–ferromagnetic term $h_\perp d_z n_1$. In turn, the profile of the Antisymmetric spiral is modified, and the expectation value of n_1 over the period L becomes nonzero and negative ($\langle n_1\rangle < 0$) in order to minimize $h_\perp d_z n_1$.

With increasing $h_\perp$, the spiral becomes significantly distorted, and the $n_1 \simeq -1$ orientation (domain) during the spin rotation is greatly enhanced. This is apparent from the bottom entry of Fig. 8(a). At the same time, the period L of the spiral increases, and the energy density of the Antisymmetric state begins to approach the energy density of the uniform Spin-flop state $\mathbf{n} = (-1, 0, 0)$ from below. At the critical value of the transverse field $h_\perp^c(h_z)$, the period of the spiral grows to infinity ($L \to \infty$), and its energy density becomes equal to the energy density of the Spin-flop state $w = \frac{1}{2}(1 - 2h_\perp d_z)$. This numerically verified scenario is consistent with the experiment[17], and is somewhat similar to that discussed in Sec. III for strictly transverse fields. Above the critical line, only the uniform Spin-flop states emerges from our numerical calculations, and the incommensurate Antisymmetric spiral no longer exists. The boundary between the Antisymmetric and the Spin-flop state is indicated by the solid line in Fig. 7. We have verified that the Antisymmetric state displayed in the phase diagram always carries lower

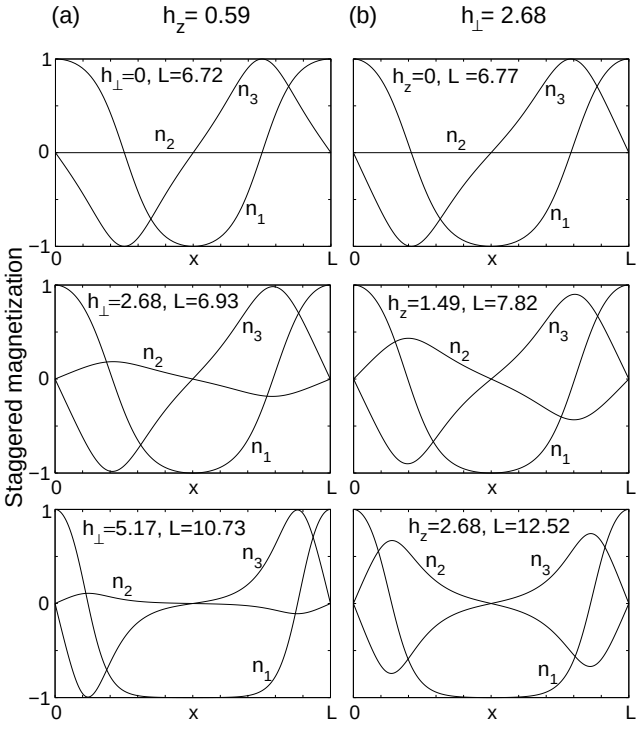

Figure 8. Calculated evolution of spin configuration in the Antisymmetric phase with the applied magnetic field. (a) Left panel: $h_z = 0.59$ ($H_z = 1$ T), $h_\perp$ increases. (b) Right panel: $h_\perp = 2.68$ ($H_\perp = 4.5$ T), h_z increases. The bottom entries in both panels are applied for points near the critical line between the Antisymmetric and the Spin-flop phase. Notice an enhanced $n_1 = -1$ domain in these entries.

energy density than the uniform Spin-flop state.

Evolution of the spin structure with increasing h_z, but fixed strength of the transverse field $h_\perp$, is shown in Fig. 8(b). Our results, applied here for $h_\perp = 2.68$ ($H_\perp = 4.5$ T), are qualitatively similar to those in Fig. 8(a). In particular, the spiral again develops a nonzero oscillating component $n_2 \neq 0$ along $h_\perp$, with zero expectation value $\langle n_2 \rangle = 0$ over the period L. Expectation value $\langle n_2 n_3 \rangle < 0$ due to the off–diagonal anisotropy $n_2 n_3 h_\perp h_z$, whereas $\langle n_1 \rangle < 0$ thanks to the weak–ferromagnetic term $h_\perp d_z n_1$. With increasing h_z, the period of the spiral L increases and presumably again diverges ($L \to \infty$) at the critical line. Above the critical line, only the uniform Spin-flop states emerges from our numerical calculations, and the incommensurate Antisymmetric spiral no longer exists.

We emphasize, that the characteristic properties of the Antisymmetric state discussed in the preceding paragraphs remain the same for *any point* $h_z \neq 0$, $h_\perp \neq 0$ below the solid line in Fig. 7. However, the scenario of the phase transition between the Antisymmetric and the Spin-flop phase, discussed in connection with Fig. 8, is slightly modified for sufficiently weak $h_\perp$, near the point Γ. Specifically, for $H_\perp$ below ~ 1 T, the energies of both states again become equal at the critical line, but the period L of the Antisymmetric spiral remains *finite* (albeit large). Above the critical line, our numerical minimization still yields the solution in the form of the Antisymmetric spiral, with however, the energy density higher than the energy density of the Spin-flop state $\mathbf{n} = (-1, 0, 0)$. This should be contrasted with behavior for large $h_\perp$, where the period of the Antisymmetric spiral *diverges* ($L \to \infty$) at the critical line; and above the critical line only the uniform Spin-flop state exists. Interestingly, our results seem to be again consistent with the experiment[17].

To complete our description of the Antisymmetric state, we display the typical 3D path traced out by the endpoint of spin during one period L in Fig. 10(c), calculated for $h_z = 1.21$ and $h_\perp = 0.28 h_z = 0.34$ ($H_z = 2.04$ T and $H_\perp = 0.57$ T). The spin approximately rotates in a plane whose normal is tilted away from the y axis in the yz plane.

To proceed further, we now explain the meaning of the dashed line in Fig. 7, and examine an important issue concerning the existence of the Spin-flop state in the presence of arbitrary canted fields. We note that the uniform Spin-flop state $\mathbf{n} = (-1, 0, 0)$, or $\Phi = -\frac{\pi}{2}$, $\Theta = \frac{\pi}{2}$ using the spherical parametrization (5), is an essentially obvious stationary point that minimizes the energy functional $W = \int V dx\, dy$, where V is the potential given in Eq. (34). Actually, there exist two different spin-flop configurations $\mathbf{n} = (\mp 1, 0, 0)$ and both of them are the stationary points of the corresponding energy functional. However, their energy densities given by $w = \frac{1}{2}(1 \mp 2 h_\perp d_z)$ are different. Therefore, we will only consider the Spin-flop state $\mathbf{n} = (-1, 0, 0)$ with lower energy in our analysis. To examine the stability, we first introduce new fields

$$\Phi(x, y, t) = -\frac{\pi}{2} + f(x, y, t)\,, \;\; \Theta(x, y, t) = \frac{\pi}{2} + g(x, y, t)\,, \tag{36}$$

where $f(x, y, t)$, $g(x, y, t)$ account for small fluctuations around the Spin-flop state. Now the actual parametrization of the staggered magnetization $\mathbf{n}$ given by Eq. (36) is inserted in the complete Lagrangian of Eq. (1), which is applied for a magnetic field $\mathbf{h}$ given by Eq. (33) and expanded to quadratic order in f, g. If we further perform the usual Fourier transformation with frequency ω and wave vector $\mathbf{q} = (q_1, q_2)$, the corresponding linearized equations of motion can be solved analytically to yield the (squared) eigenfrequencies

$$\omega_\pm^2(\mathbf{q}) = q_1^2 + q_2^2 + h_\perp d_z + \tag{37}$$

$$+ \frac{1}{2}\left(1 + h_z^2 + h_\perp^2 \pm \sqrt{\left(1 + h_z^2 - h_\perp^2\right)^2 + 4 h_z^2 h_\perp^2 + 16 q_2^2}\right).$$

The above calculated magnon spectrum is strongly anisotropic. To examine the local stability of the Spin-flop state, we note that the stability condition requires that $\omega_+^2 \geq 0$ and $\omega_-^2 \geq 0$ for each $\mathbf{q}$. It is also clear that $\omega_+^2 \geq \omega_-^2$, and ω_-^2 is minimum for $q_1 = 0$. Therefore, we

minimize ω_-^2 with respect to q_2 and then set $\omega_-^2 = 0$ to obtain

$$h_z^2 = 3 - h_\perp^2 - 2\sqrt{h_\perp^2 + 4h_\perp d_z}. \qquad (38)$$

The above obtained line of local stability of the Spin-flop state is displayed by the dashed line in the phase diagram of Fig. 7. Below the dashed line, the Spin-flop state is locally unstable. Thus the Spin-flop state cannot exist beyond the point Γ, where the energy density of the Antisymmetric state becomes equal to the energy density of the Spin-flop state.

It is more or less clear, there is a new phase realized in some area just below the dashed line, near the axis H_z (near $H_\perp = 0$). Note that Eq. (38) applied for the special case $h_\perp = 0$ yields $h_z = \sqrt{3}$ ($H_z = 2.9$ T), which is just the upper critical field h_{c2} obtained in Ref. 12. For $h_z < h_{c2}$, the Spin-flop phase is locally unstable, and the intermediate phase is realized in the region $h_{c1} < h_z < h_{c2}$. It is then natural to expect that the intermediate phase exist in some form also in the presence of a weak transverse field $h_\perp \neq 0$.

Our calculations confirms this expectation. Specifically, when $h_\perp \neq 0$, the so–called Symmetric phase emerges as the ground state in the region between the dashed and the solid line in Fig. 7. Examples of the Symmetric spiral, calculated for two values of the applied magnetic field, are illustrated in the middle and the bottom entry of Fig. 9(a). The typical path, traced out by the endpoint of the spin is shown in Fig. 10(b). The Symmetric phase can be described as an antiferromagnetic conical spiral that propagates *strictly along y*, but nutates around the $-x$ axis. Importantly, the component n_1, *perpendicular* to the transverse field $h_\perp$, is nonzero ($n_1 \neq 0$) and always negative ($\langle n_1 \rangle < 0$). All these features agree with the experiment[17].

The Symmetric phase is a direct descendant of the intermediate phase – the conical antiferromagnetic spiral– discussed in Sec. II for fields strictly parallel to c ($h_\perp = 0$). Recall that the intermediate phase obeys the U(1) symmetry described by Eq. (3). In practice, the U(1) symmetry is broken by an additional tetragonal symmetry induced by discreteness effects[6,15]. Thus, in the absence of transverse fields, there exist four degenerate states, illustrated in Fig. 10(a): the intermediate spiral propagates along x and nutates around the $\pm y$ axis; or it propagates along y but nutates around the $\mp x$ axis.

The above described degeneracy is broken when $h_\perp \neq 0$. To see that, we consider for a moment the intermediate spiral $\mathbf{n}$ calculated for $h_\perp = 0$, and insert this solution in the potential (34) applied for $h_\perp \neq 0$. The additional corrections to the energy are then given by $\frac{1}{2}h_\perp^2 \langle n_2^2 \rangle + h_\perp d_z \langle n_1 \rangle$. The first correction, quadratic in $h_\perp$, originates in the Zeeman energy $\propto (\mathbf{n} \cdot \mathbf{h})^2$. Note that the off–diagonal term $h_\perp h_z \langle n_2 n_3 \rangle$ in the Zeeman energy does not contribute, because the expectation value $\langle n_2 n_3 \rangle$ vanishes in the intermediate phase for any degenerate state. The second correction, linear in $h_\perp$, is due to the weak–ferromagnetic term $d_z(\mathbf{h} \times \mathbf{e}_3) \cdot \mathbf{n}$. The linear weak–ferromagnetic contribution dominates for small transverse field, and favors the conical spiral propagating along y and nutating around the $-x$ axis, with $\langle n_1 \rangle < 1$.

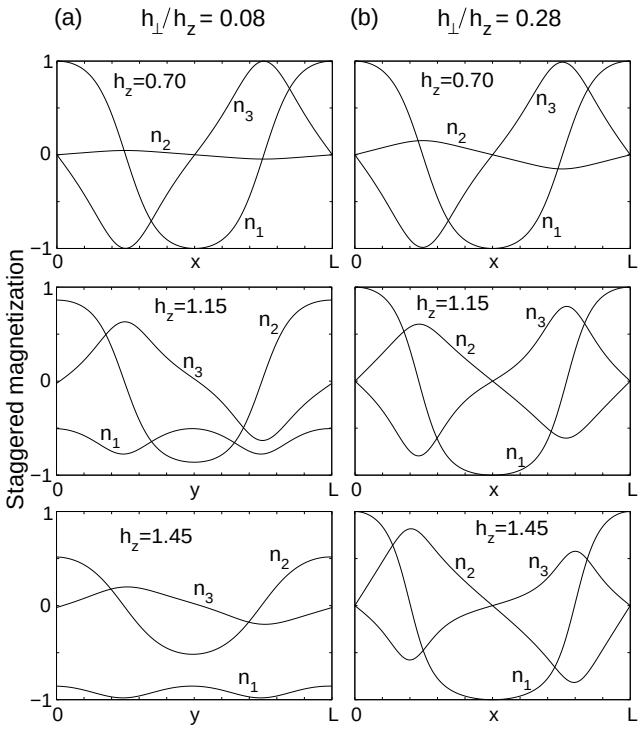

Figure 9. Examples of spin configurations in various phases from the phase diagram in Fig. 7, calculated for (a) $h_\perp/h_z$=0.08, and (b) $h_\perp/h_z$= 0.28. The two values $h_\perp/h_z$ correspond to the magnetic field applied at an angle 4.57° and 15.64° with respect to the c axis. The middle and the bottom entry in (a) corresponds to the Symmetric phase, where the spiral propagates along y. All other entries show the Antisymmetric phase, with propagation direction along x. Phase transition between the Antisymmetric and the Symmetric phase is accompanied by sudden $\pi/2$ rotation of propagation direction.

Numerical work confirms that the above argument is correct despite the simplifying assumption that neglects the changes in the staggered magnetization induced by $h_\perp \neq 0$. Thus, the Symmetric phase illustrated in Fig. 9(a) and Fig. 10(b), is essentially the intermediate phase of Sec. II, propagating along y but nutating around the $-x$ axis, whose profile $\mathbf{n}$ is modified by $h_\perp \neq 0$.

Sudden rotations

The Symmetric phase emerges in canted magnetic fields applied nearly parallel to the c axis, when $h_z \gtrsim h_{c1}$. It is the stationary point of the energy functional with the lowest energy density in the area between the dashed line and the solid line of Fig. 7. With increasing h_z the magnitude of n_1 becomes larger and larger, until at the dashed line $n_1 \to -1$ and the solution becomes the Spin-

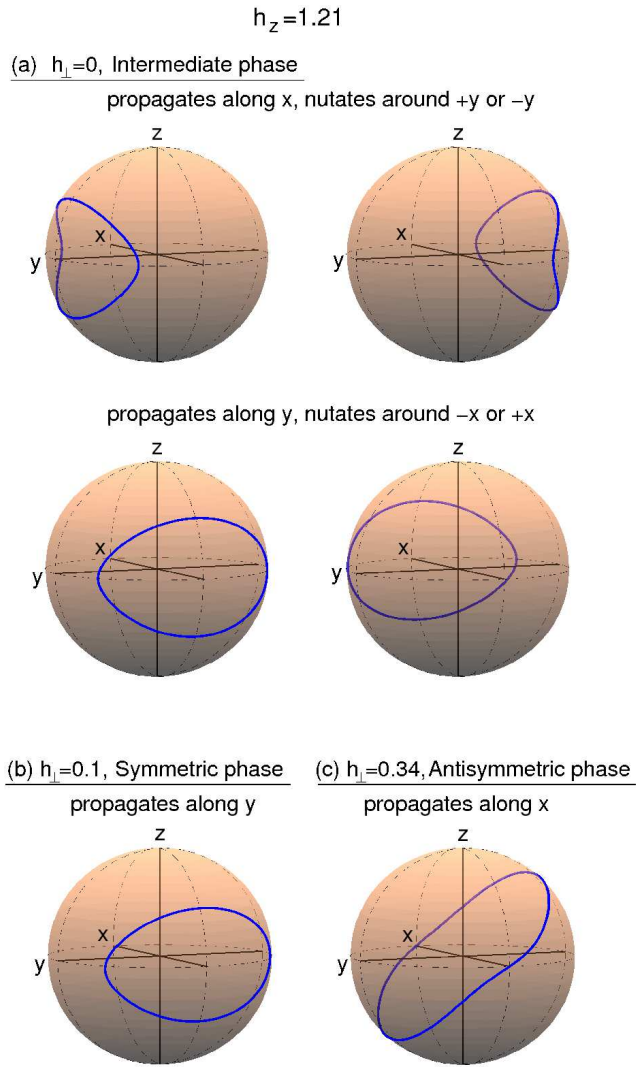

Figure 10. (Color online) Typical spin configurations in canted magnetic fields, calculated for h_z=1.21 and the three values of the transverse field $h_\perp$. Thick lines on the sphere indicate paths traced out by the endpoints of the staggered magnetization during one period L. The base of the staggered magnetization is placed at the center of the sphere. (a) Intermediate phase, $h_\perp = 0$. The conical spiral may propagate along x and nutate around the $\pm y$ axis; or may propagate along y and nutate around the $\mp x$ axis. (b) Symmetric phase, $h_\perp = 0.1$. The conical spiral propagates strictly along y but nutates around the $-x$ axis. (c) Antisymmetric phase, $h_\perp = 0.34$. Spin approximately rotates in a plane, whose normal is tilted away from the axis y in the yz-plane. The spiral propagates strictly along the x axis.

flop state $\mathbf{n} = (-1, 0, 0)$. These results generally agree with experimental findings[16,17]. Evolution of the spin structure with increasing $h_\perp$, but fixed strength of the longitudinal component h_z is rather mild. The period L slightly decreases with $h_\perp$, whereas the magnitude of n_1 moderately increases due to the weak–ferromagnetic energy $d_z(\mathbf{h} \times \mathbf{e}_3) \cdot \mathbf{n}$.

Importantly, at the critical solid line the energy density of the Symmetric phase becomes equal to the energy density of the Antisymmetric phase. For the special choice $h_z = 1.21$ shown in Fig. 10, this happens at $h_\perp \approx 0.13$ or 0.22 T. For stronger $h_\perp$, the Antisymmetric state (Fig. 10(c)) emerges as the true ground state, with the energy density lower than the Symmetric spiral .

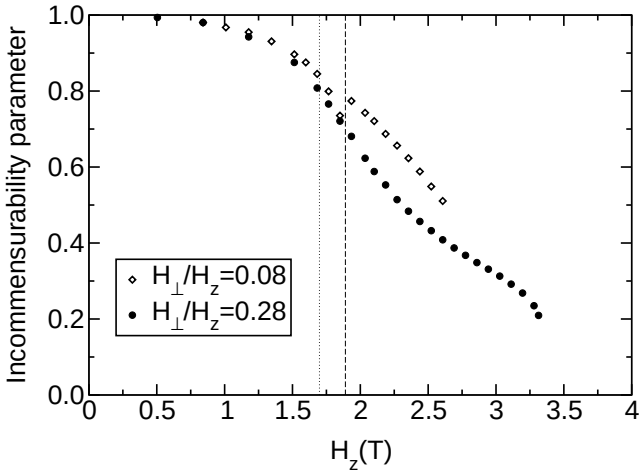

Figure 11. Theoretical field dependence of the incommensurability parameter calculated for $H_\perp/H_z$=0.08 and 0.28. The two values $H_\perp/H_z$ correspond to the magnetic field applied at an angle 4.57° and 15.64° with respect to the z-axis. Our choice closely follows values 5° and 15° used in the experimental Fig. 10, Ref. 17. The SI units are used to facilitate comparison with the experiment. For $H_\perp/H_z$=0.08, a predicted discontinuous jump of the incommensurability parameter by $\sim 5\%$ at $H_z \approx 1.89$ T (dashed line) corresponds to the phase transition between the Antisymmetric and the Symmetric phase. This is consistent with the experimental data. The dotted line corresponds to the critical field H_{c1}.

Because the Symmetric spiral propagates strictly along y, whereas the Antisymmetric phase propagates along the x axis, the above described *first order* phase transition is accompanied by a *sudden rotation of the spiral propagation direction* exactly by $\frac{\pi}{2}$. This theoretical result agrees with experiments[16,17].

In order to compare with the experiment directly, we present our results calculated for two values of the parameter $h_\perp/h_z = 0.08$ and/or 0.28, in Figs. 9, 11 and 12. Our choice of $h_\perp/h_z$ corresponds to a magnetic field applied at the angle $\alpha = 4.57°$ and 15.64° with respect to the c axis, which is similar to the angles 5° and 15° used in neutron scattering measurements[17].

Fig. 9(a) applied for fields nearly parallel to the c axis ($h_\perp/h_z = 0.08$, or $\alpha = 4.57°$), summarizes the evolution of the spin structure with increasing strength of the field across the phase transition. For $h_z = 0.70 < h_{c1}$ (the top entry), the system is in the Antisymmetric phase. The Antisymmetric spiral propagates along x, perpendicular to the transverse field $h_\perp$. Its oscillating component n_2 is for given value of the field rather small, and the structure resembles the flat spiral ($n_2 = 0$). It may be identified with the soliton lattice of Ref. 17. For $h_z \gtrsim h_{c1}$, the

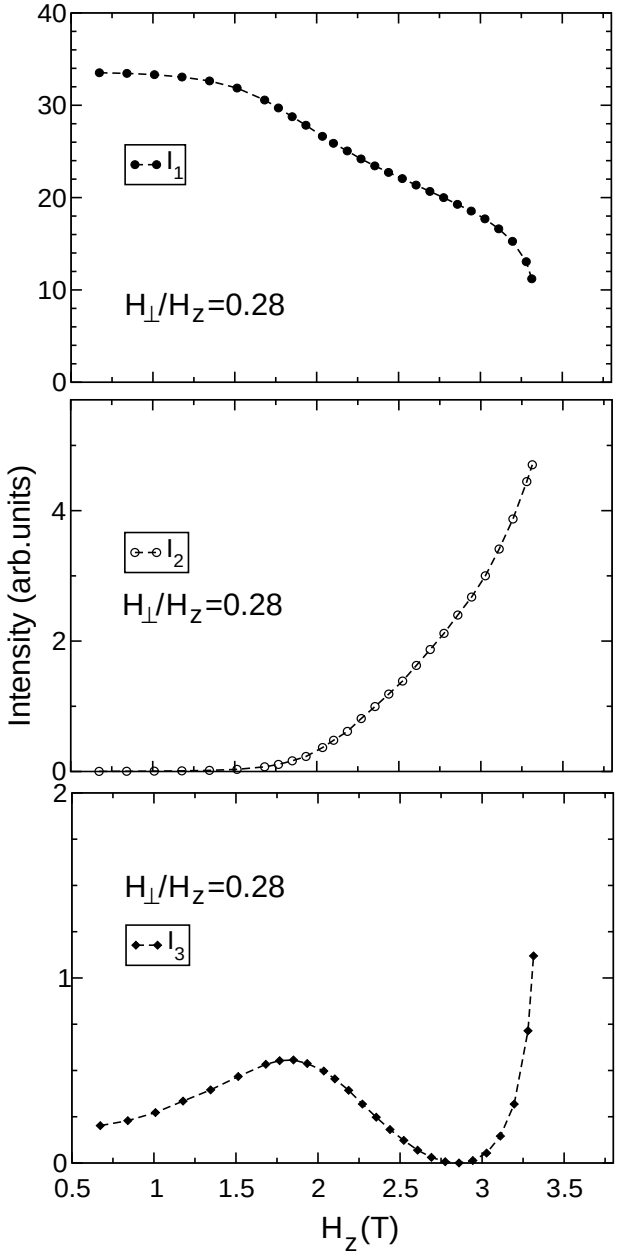

Figure 12. Theoretical field dependence for the intensities of the 1st, 2nd and the 3rd Fourier harmonics calculated from the n_1 and n_3 components of the staggered magnetization. We used $H_\perp/H_z$=0.28. The latter parameter corresponds to the magnetic field applied at an angle 15.64° with respect to the z-axis and is roughly equal to 15° used in the experimental Fig. 8, Ref. 17. We adopt SI units to facilitate comparison with the experiment.

Symmetric state - a conical structure propagating along y, but nutating around the $-x$ axis emerges (the middle and the bottom entry). Note that $h_\perp$ is applied along y, and our result is thus in agreement with Fig. 13 of Ref. 17. The Symmetric spiral should be identified with the *AF cone* of Ref. 17. The phase transition at the critical field $h_z \approx h_{c1}$ is of first order, and is accompanied by the *sudden* $\frac{\pi}{2}$ *rotation* of the spiral propagation direction. This experimental observation[16,17] is explained by our theoretical analysis. The magnitude of n_1 increases with the strength of the field, and $n_1 \to -1$ at the critical field ≈ 2.7 T. For stronger fields, the system is in the Spin-flop state. The calculated value of the IC phase transition is slightly larger than the experimental value 2.4 T.

The calculated field dependence of the incommensurability parameter $L(0)/L(h)$ is presented in Fig. 11 (empty diamonds). Note a discontinuous jump at ≈ 1.89 T where the incommensurability parameter increases by $\approx 5\%$. This corresponds to the phase transition from the Antisymmetric to the Symmetric phase and highlights its first order nature. We emphasize a remarkable agreement with experimental data in Fig. 10 of Ref. 17 and quoted values 1.95 T and $\approx 6\%$ for the critical field and a discontinuous jump of the incommensurability parameter. Actually our data are shown only for field values up to 2.6 T $< H_{c2} \approx 2.7$ T. However, our calculations indicate a continuous IC transition with $n_1 \to -1$, but *finite* L in the limit $H \to H_{c2}$.

We now discuss the case where the field is applied at "large" angle $\alpha \approx 15°$ ($h_\perp/h_z = 0.28$) with respect to the c axis. Evolution of the spin structure with increasing strength of the field is summarized in Fig. 9(b), while the corresponding field dependence of the incommensurability parameter $L(0)/L(h)$ is illustrated in Fig. 11 (full circles). In this case, no reorientation of the spiral propagation direction was observed in the experiment[17]. This is consistent with our $T = 0$ calculations, which predict the Antisymmetric phase with oscillating $n_2 \neq 0$ (*parallel* to $h_\perp$) propagating along x for all field strengths until the IC transition at ≈ 3.33 T. Predicted critical field is somewhat larger than observed in the experiment, but is not terribly inconsistent with the value 2.6 T quoted in Ref. 17. The n_2 component is small for weak fields, but its magnitude quickly increases with the strength of the field. For strong fields, the structure becomes clearly non-sinusoidal, and non-planar and can be identified with the "distorted incommensurate structure" of Ref. 17. This is seen in the middle and the bottom entry in Fig. 9(b). The Fourier transform of the staggered magnetization provides evidence for higher harmonics, both odd and even.

Our $T = 0$ theoretical results for the field dependence of the *intensities* of the 1st, 2nd and 3rd Fourier components of the staggered magnetization $\mathbf{n}(x)$ are presented in Fig. 12. The intensities are calculated from the n_1, n_3 components. This is because neutron scattering sees only the components perpendicular to momentum transfer (which is parallel to n_2). Our results are to be compared with experimental data in Fig. 8(b) of Ref. 17. For the 1st harmonic the agreement with experiment is apparent, except that we predict somewhat higher value for the of the IC critical field. Higher harmonics smoothly appear above 1.7 T - 2 T, and the intensity of 2nd harmonics linearly increases with the field, as in the experiment. Similarly, the 3rd harmonics first

increases, then shows a shallow dip and increases again close to the IC critical field. This is again fully consistent with experimental observation. On the other hand, our results show rapid increase of both higher harmonics as the field approaches the critical value, whereas the experimental data show smoothing at the IC transition. This can be perhaps due to finite temperature. Overall agreement with experiment is however fairly good. Finally we discuss the field dependence of the incommensurability parameter $L(0)/L(h)$ shown in Fig. 11 (full circles). In agreement with experiment, no discontinuous jump in the theoretical prediction is observed. The curve is concave for weak field strengths, but becomes convex for $H \gtrsim 1.7$ T. This corresponds to the emergence of higher harmonics and is again in agreement with the experimental data in Fig. 10 of Ref. 17, with minor discrepancy in the value of the IC critical field.

We end this section with two comments:

- Numerical work confirms that the existence of $d_z \neq 0$ is not crucial for the appearance of the *double-k structure* and/or sudden $\pi/2$ rotations observed in experiment. It is, however, important to restore quantitative agreement with experiment. In particular, for $d_z = 0$ and fields nearly parallel to c, the intermediate phase would first appear at h_{c1} in the form of a nonflat spiral propagating strictly along x but nutating around the y axis, *without* reorientation of the spin propagation direction. A sudden $\pi/2$ rotation of the propagation direction occurs later, at yet another critical field $h_{rotation} \approx 1.20$, above which the minimum energy state becomes the Symmetric spiral propagating along y but nutating around the x axis. In the absence of the weak–ferromagnetic energy $d_z(\mathbf{h} \times \mathbf{e}_3) \cdot \mathbf{n}$, an explanation of sudden reorientation requires a detailed analysis of the of the energy term $\propto (\mathbf{n} \cdot \mathbf{h})^2$.

- We assumed that the transverse component of the field $h_\perp$ points strictly along the y axis. Our results, however, are not restricted to this special case. For example, assume that $h_\perp$ points in an arbitrary direction in the xy plane, which is obtained by a clockwise rotation of the y axis with angle ψ. Then the staggered magnetization $\mathbf{n}$ for any state calculated earlier in this section must be also rotated clockwise with the angle ψ around the c axis, while the original direction of spin propagation must be rotated counter-clockwise, with the angle $-\psi$. All other results remain unchanged.

V. CONCLUSION

We have presented a rather complete theoretical study of $T = 0$ phase transitions in canted fields of arbitrary strength and direction. We calculated the complete phase diagram and identified the symmetries of states in a number of different regions. For the fields applied nearly parallel to the c axis, we confirmed the existence and stability of the "intermediate" phase that mediates the incommensurate-commensure transition and analyzed its properties. We identify this phase with an experimentally observed *double-k structure*. By analyzing data on fields applied perpendicular to the c axis, we determine an out-of-plane anisotropy parameter d_z needed to complete quantitative comparison with experiment. Finally, our model accounts for sudden $\pi/2$ rotations that have been highlighted as a noteworthy feature of recent experiments.

The work reported in this paper results from a long-standing theoretical investigation of spiral magnetic structures in Dzyaloshinskii-Moryia antiferromagnets. The theoretical framework involves a number of approximations: the replacement of quantum-mechanical by classical variables, ignoring inter-layer couplings and the replacement of discrete spins by continuous fields in a model Lagrangean.

Nevertheless, detailed agreement with experiment[16,17] is now so extensive that the applicability of this model to systems such as $Ba_2CuGe_2O_7$ may now be established. The only remaining discrepancies lie in the particular magnetic field values at which transitions between magnetic states take place, and these discrepancies are on the order of 10–20%, which is not much beyond experimental uncertainty.

ACKNOWLEDGMENTS

This work was partially supported by ESF Research Networking Programme POLATOM. J.C. gratefully acknowledges the support by the Slovak Research and Development Agency under the contract No. APVV-0027-11. M.M. acknowledges partial support also from the U.S. National Science Foundation through DMR1002428. The work of N.P. has been co-financed by the European Union (European Social Fund, ESF) and Greek national funds through the operational program Education and Lifelong Learning of the National Strategic Reference Framework (NSRF) under "Funding of proposals that have received a positive evaluation in the 3rd and 4th Call of ERC Grant Schemes".

* Jaroslav.Chovan@umb.sk
† marder@mail.texas.edu
‡ papanico@physics.uoc.gr

[1] I. E. Dzyaloshinskii, Sov. Phys. JETP **5**, 1259 (1957).
[2] T. Moriya, Phys. Rev. Lett. **4**, 228 (1960).

[3] A. Zheludev, G. Shirane, Y. Sasago, N. Koide, and K. Uchinokura, Phys. Rev. B **54**, 15163 (1996).
[4] A. Zheludev, S. Maslov, G. Shirane, Y. Sasago, N. Koide, and K. Uchinokura, Phys. Rev. B **57**, 2968 (1998).
[5] A. Zheludev, S. Maslov, G. Shirane, I. Tsukada, T. Masuda, K. Uchinokura, I. Zaliznyak, R. Erwin, and L. P. Regnault, Phys. Rev. B **59**, 11432 (1999).
[6] A. Zheludev, S. Maslov, G. Shirane, Y. Sasago, N. Koide, and K. Uchinokura, D. A. Tennant, and S. E. Nagler, Phys. Rev. B **56**, 14006 (1997).
[7] A. Zheludev, S. Maslov, G. Shirane, Y. Sasago, N. Koide, and K. Uchinokura, Phys. Rev. Lett. **78**, 4857 (1997).
[8] I. E. Dzyaloshinskii, Sov. Phys. JETP **20**, 665 (1965).
[9] P. G. de Gennes, Solid State Comm. **6**, 163 (1968).
[10] R. B. Meyer, Appl. Phys. Lett. **14**, 208 (1969).
[11] P. G. de Gennes and J. Prost, *The Physics of Liquid Crystals*, (Clarendon Press, Oxford, 1995).
[12] J. Chovan, N. Papanicolaou and S. Komineas, Phys. Rev. B **65**, 064433 (2002).
[13] J. Chovan, Ph.D. thesis, P. J. Šafárik University, Košice (2002).
[14] J. Chovan and N. Papanicolaou, *Frontiers in Magnetic Materials*, p.347-384, Ed. A. N. Narlikar (Springer-Verlag, Berlin Heidelberg, 2005).
[15] J. Chovan and N. Papanicolaou, Ukr. J. Phys. **50**, 747 (2005); arXiv:cond-mat/0504262.
[16] S. Mühlbauer, S. N. Gvasaliya, E. Pomjakushina, and A. Zheludev, Phys. Rev. B **84**, 180406(R) (2011).
[17] S. Mühlbauer, S. N. Gvasaliya, E. Ressouche, E. Pomjakushina, and A. Zheludev, Phys. Rev. B **86**, 024417 (2012).